Supporting Information

A platinum nanoparticle doped self-assembled peptide bolaamphiphile hydrogel as an efficient electrocatalyst for the hydrogen evolution reaction

Deepak K. K. Kori, Rohit G. Jadhav, Likhi Dhruv, Apurba K. Das*

Department of Chemistry and Centre for Advanced Electronics (CAE), Indian Institute of Technology Indore, Indore 453552, India

E-mail: apurba.das@iiti.ac.in

Table of Content

Sr. No.	Description	Page No.
1	**Materials and methods** Material Characterization Synthetic procedure	S4
2	**Table S1**. Formation of Pt NPs doped peptide bolaamphiphile hydrogels	S9
3	**Figure S1**. Snapshot of inverted vials of Pt NPs doped peptide bolaamphiphile hydrogels.	S10
4	**Figure S2.** Calibration curve of Ag/AgCl reference electrode in (a) 0.1 M H_2SO_4; (b) 0.5 M H_2SO_4; (c) 1 M H_2SO_4 with respect to reversible hydrogen electrode.	S10
5	**Figure S3.** Emission spectrum of hydrogel (λ_{ex} = 280 nm).	S11
6	**Figure S4.** Amplitude strain sweep experiment (at constant frequency 1 rad s^{-1}) of hydrogel at pH 8.0.	S11
7	**Figure S5.** (a) XPS survey profile of hydrogel with the high-resolution profile of (b) C 1s, (c) O 1s	S12
8	**Figure S6**. (a) iR-corrected LSV profiles of Pt2@hydrogel/CP, Pt4@hydrogel/CP, Pt6@hydrogel/CP, Pt8@hydrogel/CP scanned at 2 mV s^{-1} in 0.5 M H_2SO_4, (b) respective Tafel slopes. (c) Nyquist plots of the prepared electrodes measured at a potential of -0.45 V.	S13
9	**Figure S7.** CV profiles of Pt2@hydrogel/CP, Pt4@hydrogel/CP, Pt6@hydrogel/CP, Pt8@hydrogel/CP at different scan rate in 0.5 M H_2SO_4 solution.	S14
10	**Figure S8.** Linear relationship between capacitive current density at 0.38 V (vs RHE) and scan rate.	S15
11	**Figure S9.** LSV profile of Pt6@hydrogel/CP before and after the stability test in 0.5 M H_2SO_4 solution.	S15
12	**Figure S10.** FE-SEM images of (a) Bare carbon paper; (b) Pt6@hydrogel/CP before stability test; (c) Pt6@hydrogel/CP after stability test.	S16
13	**Figure S11.** (a) XPS survey profile of Pt6@hydrogel/CP with the high-resolution profile of (b) O 1s, (c) C 1s, (d) Pt 4f after stability test.	S16
14	**Figure S12.** CV profiles of Pt6@hydrogel/CP, 10% Pt/C, Pt NPs/CP, and hydrogel/CP at different scan rate in 0.5 M H_2SO_4 solution.	S17
15	**Figure S13.** Linear relationship between capacitive current density at 0.38 V (vs RHE) and scan rate.	S18
16	**Figure S14**. (a) iR-corrected LSV profiles of Pt6@hydrogel/CP scanned at 2 mV s^{-1} in 0.1 M H_2SO_4 and 1 M H_2SO_4, (b) respective Tafel slopes.	S18

17	**Figure S15**. (a) iR-corrected LSV profiles of carbon paper (CP), hydrogel/CP, Pt NPs/CP, Pt6@hydrogel/CP and 10% Pt/C scanned at 2 mV s^{-1} in 1 M KOH solution, (b) respective Tafel slopes. (c) Nyquist plots of the prepared electrodes measured at a potential of -0.45 V. (d) The chronopotentiometry analysis of Pt6@hydrogel/CP for 5 h in 1 M KOH.	S19
18	**Figure S16**. (a) iR-corrected LSV profiles of carbon paper (CP), hydrogel/CP, Pt NPs/CP, Pt6@hydrogel/CP and 10% Pt/C scanned at 2 mV s^{-1} in 1 M Phosphate buffer solution, (b) respective Tafel slopes. (c) Nyquist plots of the prepared electrodes measured at a potential of -0.45 V. (d) The chronopotentiometry analysis of Pt6@hydrogel/CP for 5 h in 1 M Phosphate buffer.	S20
19	**Table S2.** HER performance of Pt2@hydrogel/CP, Pt4@hydrogel/CP, Pt6@hydrogel/CP, Pt8@hydrogel/CP in 0.5 M H_2SO_4 solution.	S21
20	**Table S3.** HER performance of Pt6@hydrogel/CP, Pt NPs/CP and Pt/C in 0.5 M H_2SO_4 solution.	S21
21	**Table S4.** Comparative HER performance of Pt-based developed electrocatalysts.	S22
22	**Table S5.** HER performance of Pt6@hydrogel/CP, in 0.1 M H_2SO_4 and 1 M H_2SO_4 solution.	S23
23	**Table S6.** HER performance of Pt6@hydrogel/CP, Pt NPs/CP and Pt/C in 1 M KOH solution.	S23
24	**Table S7.** HER performance of Pt6@hydrogel/CP, Pt NPs/CP and Pt/C in 1 M Phosphate buffer solution.	S23
25	^{1}H NMR and ^{13}C NMR data of all compounds.	S24
26	Mass spectrometry data of all compounds.	S29

Materials and methods

Materials

Glutaric acid, 1-hydroxybenzotriazole (HOBt), amino acids and *N*,*N*'-diisopropylcarbodiimide (DIC) were purchased from SRL chemicals, India and used without further purification. Potassium tetrachloroplatinate (II) (K_2PtCl_4) was purchased from SD Fine-Chem. Ltd. Nafion-117 solution was purchased from Sigma Aldrich Chemicals. Carbon paper was obtained from Global Nanotech, Mumbai, India. All solvents were analytical grade, purchased from Merck chemicals and distilled before use. Milli-Q water was used in all experiments.

Characterization methods

^{1}H and ^{13}C NMR spectra of all the precursors and final compound were recorded on Bruker AV 400 MHz instrument using tetramethylsilane as the internal standard and DMSO-*d*6 as solvent. The concentration of the compound was between 8-10 mmol. Mass spectra were recorded on a Bruker Daltonic LC-MS spectrometer by positive mode electron spray ionizations. FTIR spectra of the compound and xerogel were acquired on Bruker (tensor 27) FT-IR spectrometer using KBr pallet method. Fluorescence spectrum of the corresponding hydrogel (20 mmol L^{-1}) was acquired on a Horiba Scientific Fluoromax-4 spectrometer with a 1 cm path length quartz cell at room temperature. X-ray photoelectron spectroscopy (XPS) measurement was carried out to determine the surface chemical state and elemental composition of the Pt@hydrogel by PHI 5000 VersaProbe III. UV-Vis absorption spectra of the hydrogel, Pt@hydrogel and K_2PtCl_4 were recorded on Jasco V 750 instrument. Mechanical and viscoelastic properties of the self-assembled hydrogel and Pt@hydrogel were obtained by performing rheological experiment using Anton Paar Physica MCR 301 rheometer at 25 ºC. Morphological studies were carried out by FE-SEM and HR-TEM. Field emission scanning electron microscopic images were obtained using a Supra55 Zeiss. Further, high-resolution transmission electron microscopic images were obtained using a JEOL JEM 2100F.

Synthetic Procedure

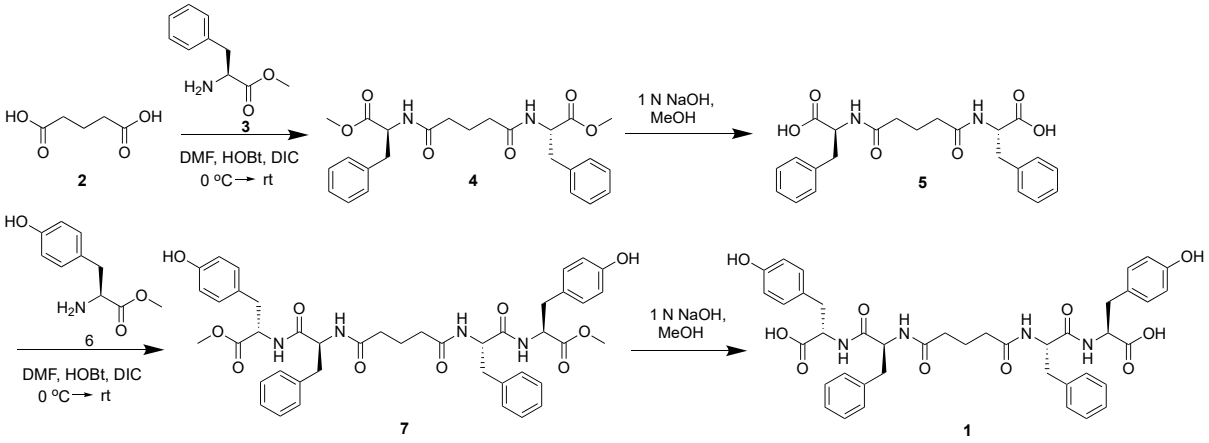

Scheme S1. Synthetic scheme for solution phase synthesis of peptide bolaamphiphile **1** (HO-Y-F-GluA-F-Y-OH)

Synthesis of MeO-F-GluA-F-OMe (4): 0.5 g (3.78 mmol) Glutaric acid was stirred with 3 mL DMF at 0 ºC followed by addition of 1.02 g (7.56 mmol) HOBt. Soon after, 2.44 g (11.34 mmol) L-phenylalanine methyl ester (**3**) was isolated from its corresponding hydrochloride salt and concentrated to add to the reaction mixture with subsequent addition of diisopropylcarbodiimide (1.04 g, 1 mL 300 µL, 8.31 mmol). The reaction mixture was left overnight. Thereafter, reaction mixture was diluted by adding 50 mL ethyl acetate and the DIU was filtered off. The organic layer was washed with 1M HCl (3X50 mL), brine (2x50 mL), 1M Na_2CO_3 (3X50 mL), brine (2x50 mL) and dried over anhydride Na_2SO_4 and evaporated under vacuum to yield (**4)** as white solid. Purification was done by flash chromatography on silica gel (100-200 mesh) using ethyl acetate: hexane (9:1) as an eluent.
Yield: 1.51 g (87%); ^{1}H NMR (400 MHz, DMSO-d_6): δ = 8.24 (d, J = 7.6 Hz, 2H, NH of Phe), 7.28 – 7.18 (m, 10H, aromatic Hs of Phe), 4.44 (d, J = 6.0 Hz, 2H, C^{α} H of Phe), 3.59 (s, 6H, OCH_3), 3.03-2.98 (m, 2H, C^{β} Hs of Phe), 2.89 – 2.83 (m, 2H, C^{β} Hs of Phe), 1.99 (d, J = 4.4 Hz, 4H, –CH_2 of Glu), 1.57 – 1.53 (m, 2H, –CH_2 of Glu). ^{13}C NMR (100 MHz, DMSO-d_6), δ = 172.71, 172.43, 137.79, 129.50, 128.71, 127.01, 53.95, 52.28, 37.16, 34.77, 21.76.
MS (ESI): *m/z* $[M+H]^+$ calculated for $C_{25}H_{30}N_2O_6$: 455.2176; found: 455.2306.

Synthesis of HO-F-GluA-F-OH (5): 0.7 g (1.54 mmol) of MeO-F-GluA-F-OMe (**4**) was taken in a round bottom flask and 10 mL MeOH was added to it. In the given reaction mixture, 5 mL 1M NaOH was added and the progress of the hydrolysis was monitored using thin layer chromatography. The reaction mixture was stirred for 5 h. Once the reaction was

complete, MeOH was evaporated under vacuum and 20 mL distilled water was added to it. Then, aqueous layer was washed with diethyl ether (2x30 mL). Furthermore, aqueous layer was collected and kept under ice cold condition and drop-wise 1M HCl was added to adjust the pH 2. Soon after, aqueous layer was extracted with ethyl acetate (3x50 mL) and dried over anhydride Na_2SO_4 and evaporated under vacuum to yield (**5)** as white solid.
Yield: 0.51 g (76%); ^{1}H NMR (400 MHz, DMSO-d_6): δ = 8.07 (d, J = 8.0 Hz, 2H, NH of Phe), 7.27 – 7.15 (m, 10H, aromatic Hs of Phe), 4.41 (d, J = 4.3 Hz, 2H, C$^\alpha$ H of Phe), 3.06 – 3.01(m, 2H, C$^\beta$ Hs of Phe), 2.85 – 2.79(m, 2 H, C$^\beta$ Hs of Phe), 1.98 – 1.95 (m, 4H, -CH_2 of Glu), 1.58-1.53 (m, 2H, –CH_2 of Glu). ^{13}C NMR (100 MHz, DMSO-d_6), δ = 173.79, 172.34, 138.18, 129.52, 128.64, 126.87, 53.82, 37.19, 34.88, 21.94, 20.72; MS (ESI): *m/z* $[M+Na]^+$ calculated for $C_{23}H_{26}N_2O_6$: 449.1683; found: 449.1652.

Synthesis of MeO-Y-F-GluA-F-Y-OMe (7): 0.5 g (1.17 mmol) MeO-Y-F-GluA-F-Y-OMe **(7)** was stirred with 3 mL DMF at 0 °C followed by addition of 0.3167 g (2.34 mmol) HOBt. Soon after, 0.81 g (3.51 mmol) L-tyrosine methyl ester was isolated from its corresponding hydrochloride salt and concentrated to add to the reaction mixture with subsequent addition of diisopropylcarbodiimide (0.32 g, 0.4 mL, 2.57 mmol). The reaction mixture was left overnight. Thereafter, reaction mixture was diluted by adding 50 mL ethyl acetate and DIU was filtered off. The organic layer was washed with 1M HCl (3X50 mL), brine (2x50 mL), 1M Na_2CO_3 (3X50 mL), brine (2x50 mL) and dried over anhydride Na_2SO_4 and evaporated under vacuum to yield **(7)** as white solid. Purification was done by flash chromatography on silica gel (100-200 mesh) using ethyl acetate: hexane (9:1) as an eluent.
Yield: 0.78 g (86%); ^{1}H NMR (400 MHz, DMSO-d_6): δ = 9.24 (s, 2H, OH of Tyr), 8.75 (d, J = 6.8 Hz, 2H, NH of Tyr), 8.36 (d, J = 8.2 Hz, 2H, NH of Phe), 7.31 – 7.15 (m, 10H, aromatic Hs of Phe), 7.04 (d, J = 8.0 Hz, 4H, aromatic Hs of Tyr), 6.67 (d, J = 8.0 Hz, 4H, aromatic Hs of Tyr), 4.55 (t, J = 8.0 Hz, 2H, C$^\alpha$ H of Tyr), 4.46-4.41 (m, 2H, C$^\alpha$ H of Phe), 3.54 (s, 6H, OCH_3), 3.01-2.91 (m, 4H, C$^\beta$ Hs of Tyr and 2H, C$^\beta$ Hs of Phe), 2.64 (t, J = 12.4 Hz, 2H, C$^\beta$ Hs of Phe), 1.88 – 1.76 (m, 4H, –CH_2 of Glu), 1.55 (d, J = 6.0 Hz, 2H, –CH_2 of Glu); ^{13}C NMR (100 MHz, DMSO-d_6): δ = 173.65, 172.50, 156.57, 138.45, 130.52, 129.66, 128.53, 127.39, 126.82, 115.59, 54.92, 54.53, 52.28, 37.88, 36.36, 34.11, 22.34; MS (ESI): *m/z* $[M+H]^+$ calculated for $C_{43}H_{48}N_4O_{10}$: 781.3443; found: 781.3314.

Synthesis of HO-Y-F-GluA-F-Y-OH (1): 0.5 g (0.64 mmol) of MeO-Y-F-GluA-F-Y-OMe **(c)** was taken in a round bottom flask and 8 mL MeOH was added to it. In the given reaction mixture, 5 mL of 1M NaOH was added and the progress of the hydrolysis was monitored using thin layer chromatography. The reaction mixture was stirred for 5 h. Once the reaction was completed, MeOH was evaporated under vacuum and 10 mL distilled water was added to it. Then, aqueous layer was washed with diethyl ether (2x30 mL). Furthermore, aqueous layer was collected and kept under ice cold condition and drop wise 1M HCl was added to adjust the pH 2. Soon after, aqueous layer was extracted with ethyl acetate (3x50 mL) and dried over anhydride Na_2SO_4 and evaporated under vacuum to yield (**1**) as white solid.
Yield: 0.31 g (65%); ^{1}H NMR (400 MHz, DMSO-d_6): δ = 12.70 (s, br, 2H, COOH), 9.21 (s, 2H, OH of Tyr), 8.54 (d, J = 5.4 Hz, 2H, NH of Tyr), 8.34 (d, J = 7.5 Hz, 2H, NH of Phe), 7.32 – 7.15 (m, 10H, aromatic Hs of Phe), 7.06 (d, J = 7.3 Hz, 4H, aromatic Hs of Tyr), 6.66 (d, J = 7.3 Hz, 4H, aromatic Hs of Tyr), 4.56 (s, 2H, C^{α}H of Tyr), 4.41 (d, J = 5.3 Hz, 2H, C^{α}H of Phe), 3.03 – 2.96 (m, 4H, C^{β} Hs of Tyr), 2.89 – 2.84 (m, 2H, C^{β} Hs of Phe), 2.68 – 2.59 (m, 2H, C^{β} Hs of Phe), 1.81 (s, 4H, –CH_2 of Glu), 1.53 (s, 2H, –CH_2 of Glu); ^{13}C NMR (100 MHz, DMSO-d_6), δ = 173.46, 172.38, 156.45, 138.44, 130.55, 129.74, 128.53, 127.82, 126.73, 115.51, 54.68, 37.89, 36.39, 34.14, 22.27; MS (ESI): *m/z* $[M+Na]^+$ calculated for $C_{41}H_{44}N_4O_{10}$: 775.2949; found: 775.3089.

Morphological study of Hydrogel and Pt@hydrogel

Transmission electron microscopy (TEM) measurements were carried out to investigate the morphology of self-assembled hydrogel and Pt@hydrogel . TEM images were acquired by using JEOL JEM 2100F with an accelerating voltage of 300 kV. In the experiment, 50 µL of hydrogel (20 mM) was added in the micro centrifuge tube containing 450 µL DI water. Then, 20 µL of diluted solution was pipetted onto a carbon-coated copper grid (300 mesh) and allowed to dry by slow evaporation in the air and separately under reduced pressure at room temperature. Phosphotungstic acid (2% w/v) was used as a negative agent for hydrogel. Field emission Gun-scanning electron microscopic experiments were conducted by using Carl Zeiss scanning electron microscope (FE-SEM Supra 55 Zeiss). A portion of 100 µL of hydrogel (20 mM) was diluted with 500 µL DI water and then 20 µL was pipetted onto a glass coverslip. Further, the glass coverslips were allowed to dry in air and then under vacuum overnight. The glass coverslips were coated with copper and the images were recorded with an operating voltage of 5 kV.

Rheological Study

Rheological analyses were performed to evaluate the mechanical properties of hydrogels by Anton Paar Physica MCR 301 Rheometer with a parallel plate-geometry (diameter: 25 mm, trugap: 0.5 mm). Hydrogel and Pt@hydrogel were transferred onto a rheometer plate by using a microspatula and kept hydrated by using a solvent trap. The dynamic strain sweep measurements were conducted to determine the region of deformation in which linear viscoelasticity is valid. Linear viscoelastic regime (LVR) was used to determine the exact strain of self-assembled hydrogel and Pt@hydrogel at a constant frequency of 10 rad s^{-1}. The mechanical strength of hydrogel and Pt@hydrogel were evaluated by performing dynamic frequency sweep measurements in the frequency range of 0.5-100 rad s^{-1} with a constant strain value of 1%.

Synthesis of Pt NPs

Pt nanoparticles were synthesised using previously reported procedures.[1,2] In a typical process, 30 µL freshly prepared aqueous solution of K_2PtCl_4 (0.1 M) was mixed with 3 mL deionized water, followed by the addition of 60 µL polyvinylpyrrolidone (0.6 M) as a stabilizing agent. The mixture was allowed to stir for 30 minutes. Subsequently, 150 µL of freshly prepared $NaBH_4$ (0.1 M) was slowly added to the system under vigorous stirring. The reaction mixture was stirred for an additional 2 h, after which colour change was observed from dark brown to black, which indicated the formation of Pt nanoparticles. Furthermore, product was centrifuged at 12000 rpm for 10 min and then the supernatant was decanted and product was collected. To obtain pure Pt nanoparticles the precipitate was washed with 10 mL acetone several times and centrifuged at 12000 rpm.

Table S1. Formation of Pt NPs doped peptide bolaamphiphile hydrogels.

Peptide Bolaamphiphile (mg)	K_2PtCl_4 (mg)	Conc. of Compound (mM)	Buffer Strength (mM)	pH	Volume of Buffer (mL)	Gelation	Images
15	2	20	20	8.0	1	Yes	 **Pt2@hydrogel**
15	4	20	20	8.0	1	Yes	 **Pt4@hydrogel**
15	6	20	20	8.0	1	Yes	 **Pt6@hydrogel**
15	8	20	20	8.0	1	Yes	 **Pt8@hydrogel**

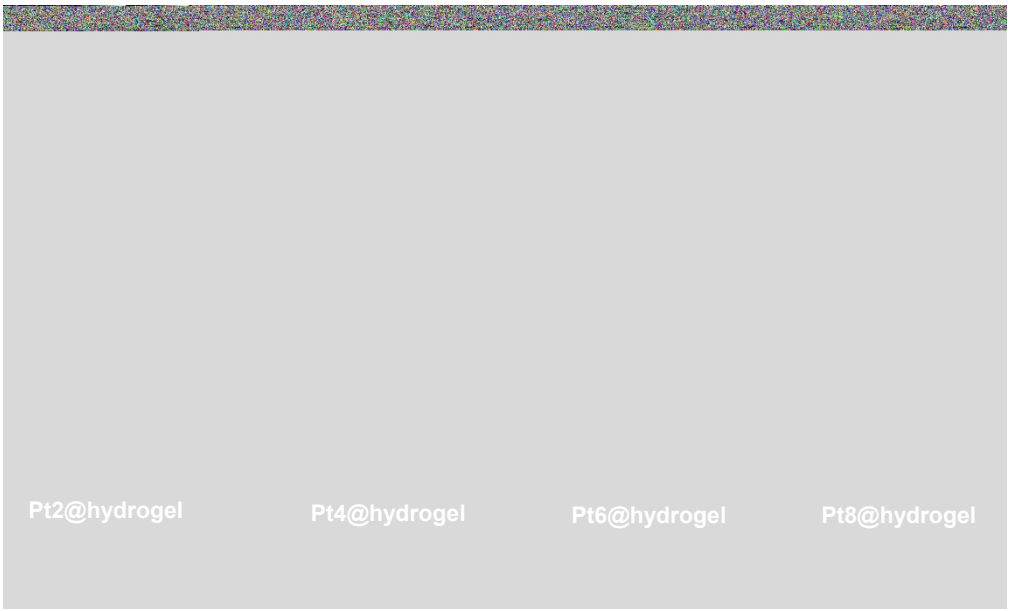

Figure **S1**. Snapshot of inverted vials of Pt NPs doped peptide bolaamphiphile hydrogels.

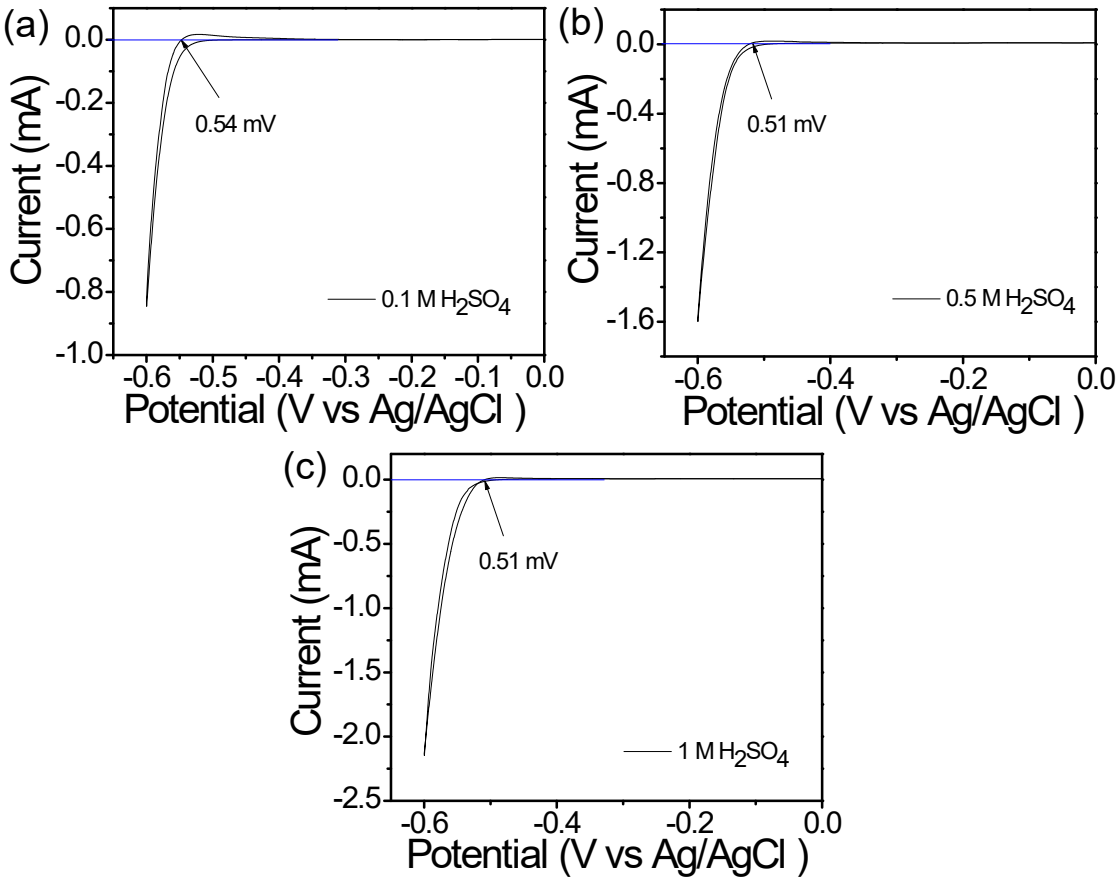

Figure S2. Calibration curve of Ag/AgCl reference electrode in (a) 0.1 M H_2SO_4; (b) 0.5 M H_2SO_4; (c) 1 M H_2SO_4 with respect to reversible hydrogen electrode.

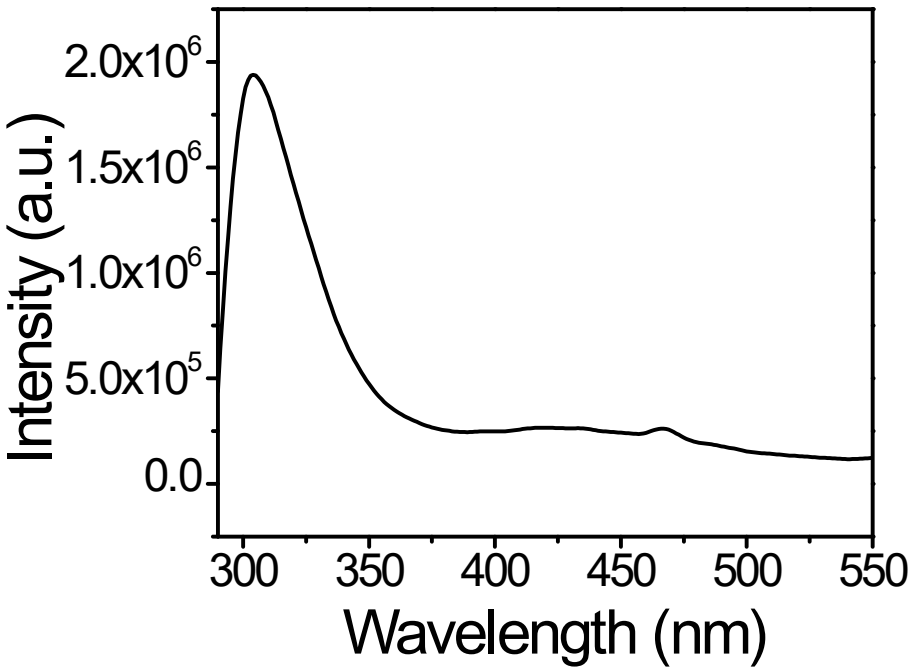

Figure S3. Emission spectrum of hydrogel (λ_{ex} = 280 nm).

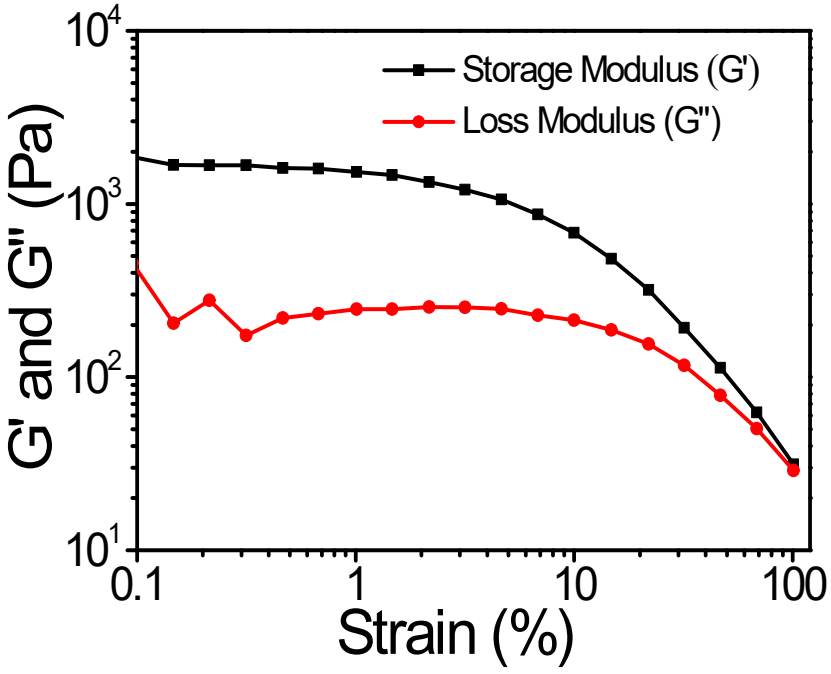

Figure S4. Amplitude strain sweep experiment (at constant frequency 1 rad s^{-1}) of hydrogel at pH 8.0.

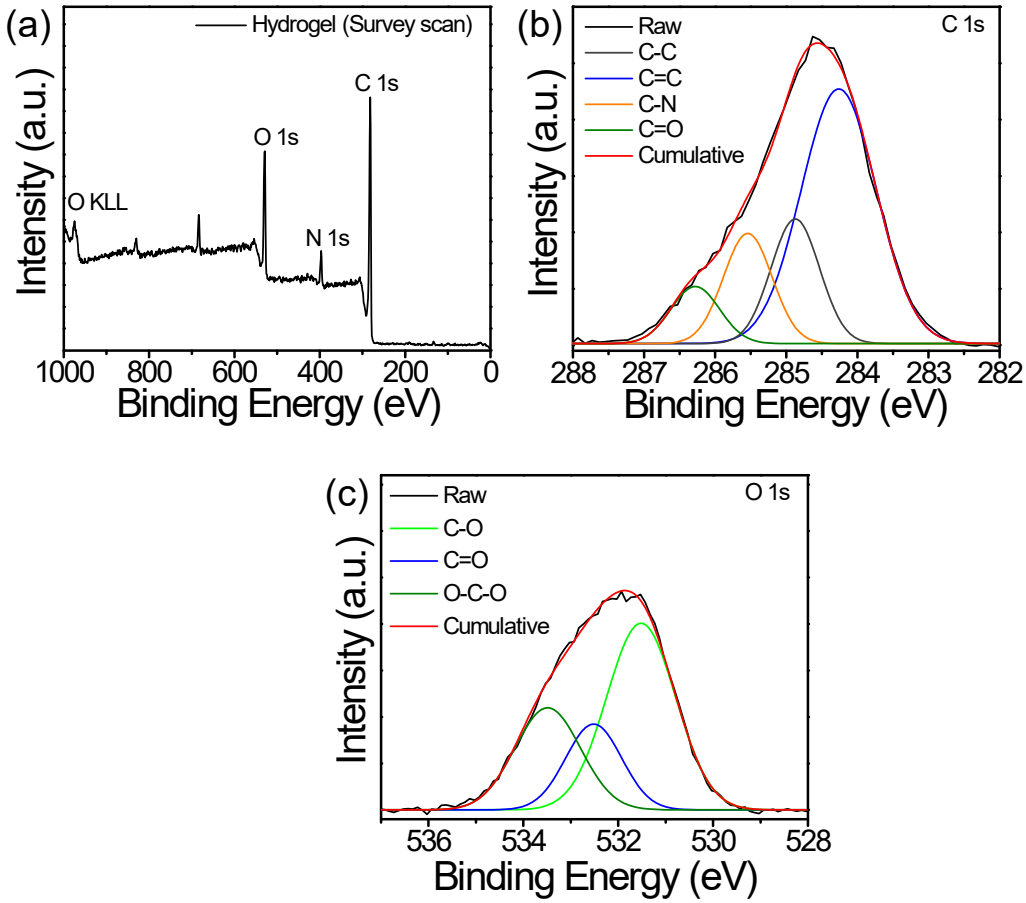

Figure S5. (a) XPS survey profile of hydrogel with the high-resolution profile of (b) C 1s, (c) O 1s.

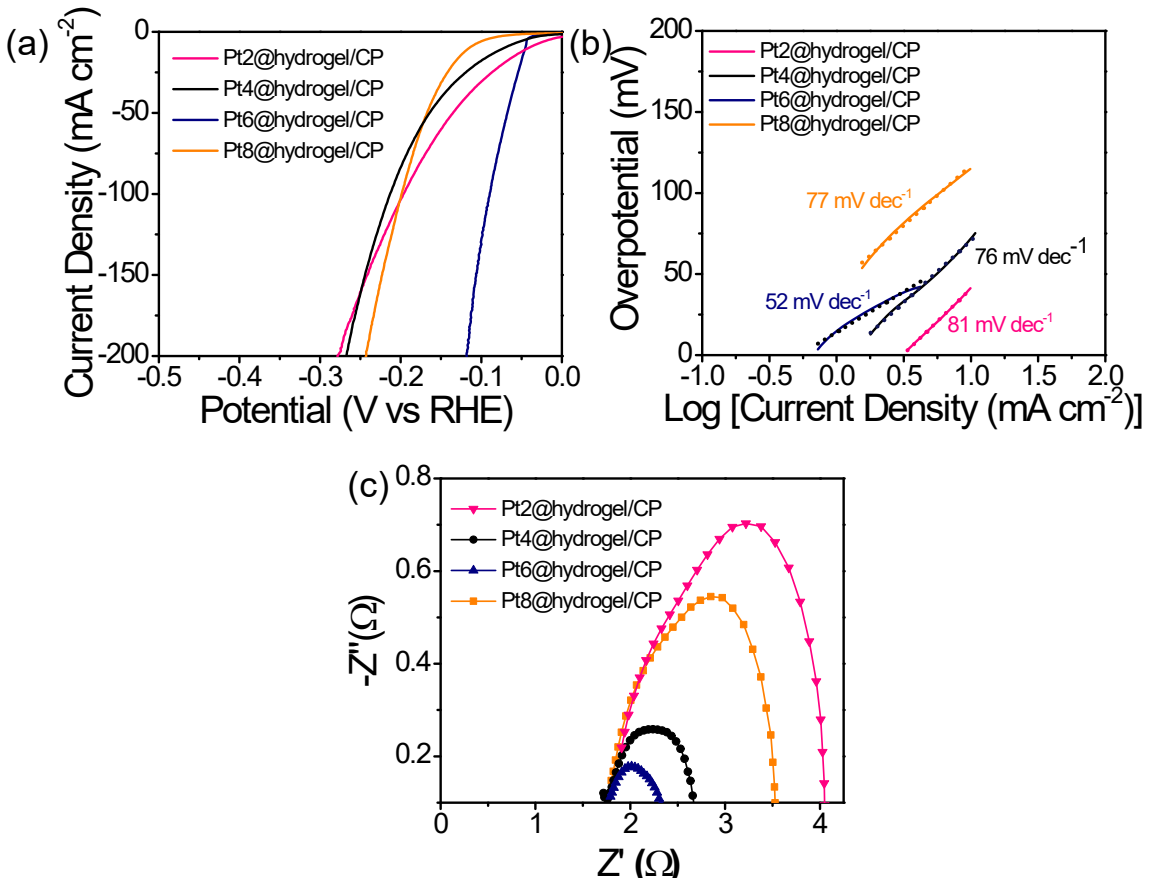

Figure S6. (a) iR-corrected LSV profiles of Pt2@hydrogel/CP, Pt4@hydrogel/CP, Pt6@hydrogel/CP, Pt8@hydrogel/CP scanned at 2 mV s^{-1} in 0.5 M H_2SO_4, (b) respective Tafel slopes. (c) Nyquist plots of the prepared electrodes measured at a potential of -0.45 V.

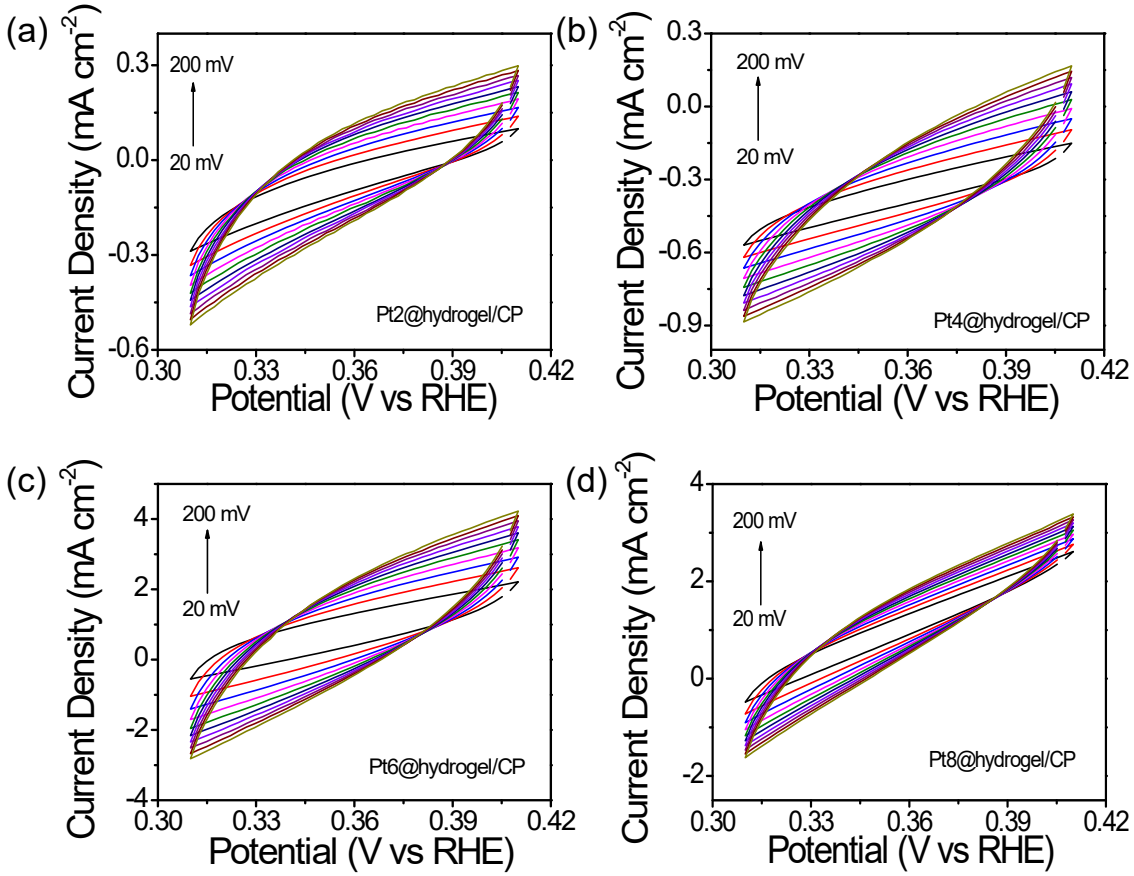

Figure S7. CV profiles of Pt2@hydrogel/CP, Pt4@hydrogel/CP, Pt6@hydrogel/CP, Pt8@hydrogel/CP at different scan rate in 0.5 M H_2SO_4 solution.

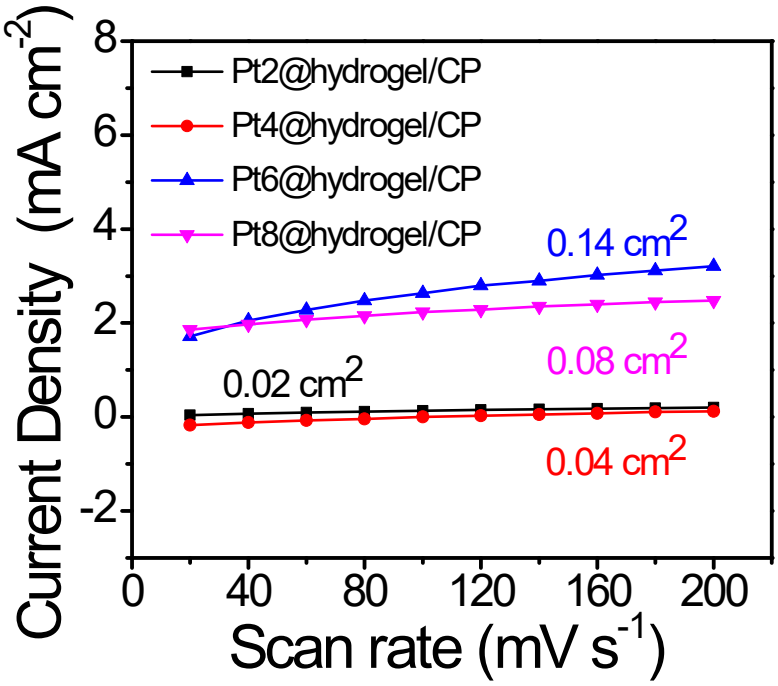

Figure S8. Linear relationship between capacitive current density at 0.38 V (vs RHE) and scan rate.

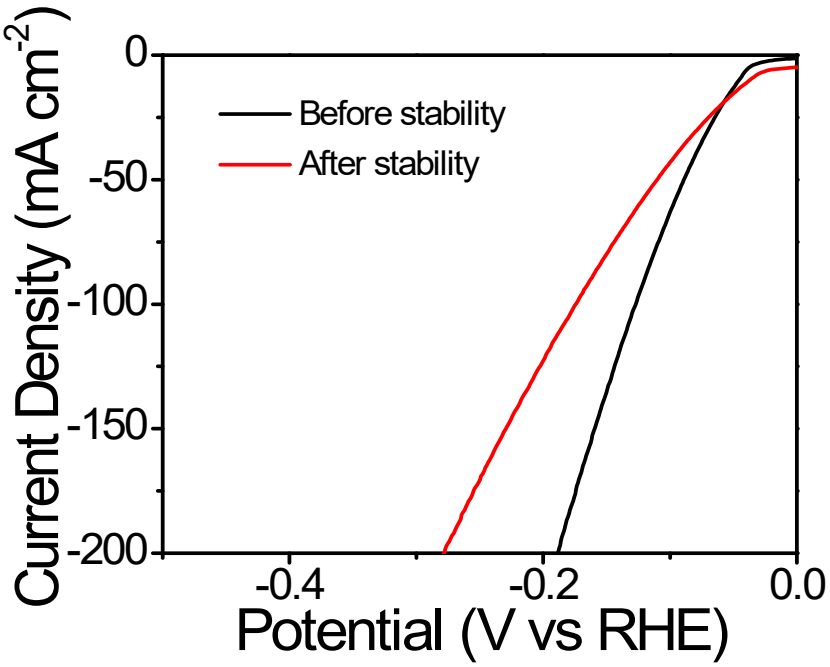

Figure S9. LSV profile of Pt6@hydrogel/CP before and after the stability test in 0.5 M H_2SO_4 solution.

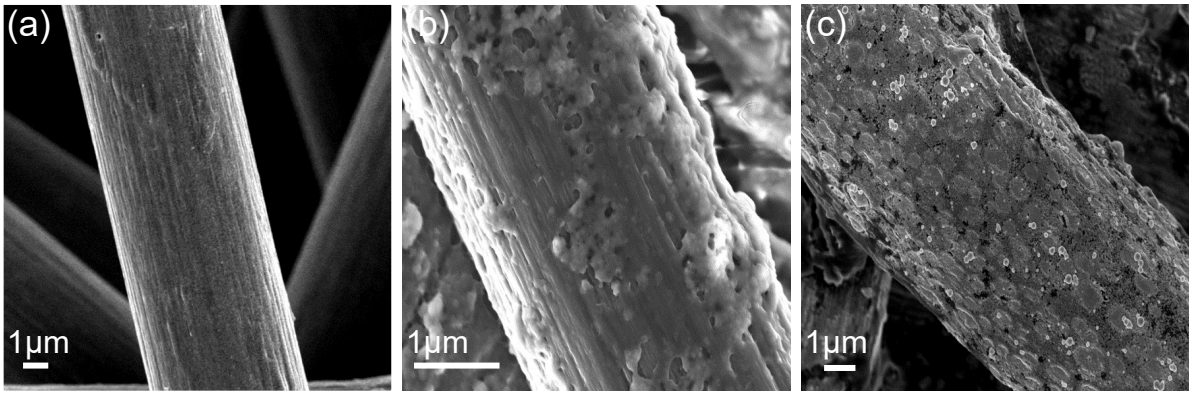

Figure S10. FE-SEM images of (a) Bare carbon paper; (b) Pt6@hydrogel/CP before stability test; (c) Pt6@hydrogel/CP after stability test.

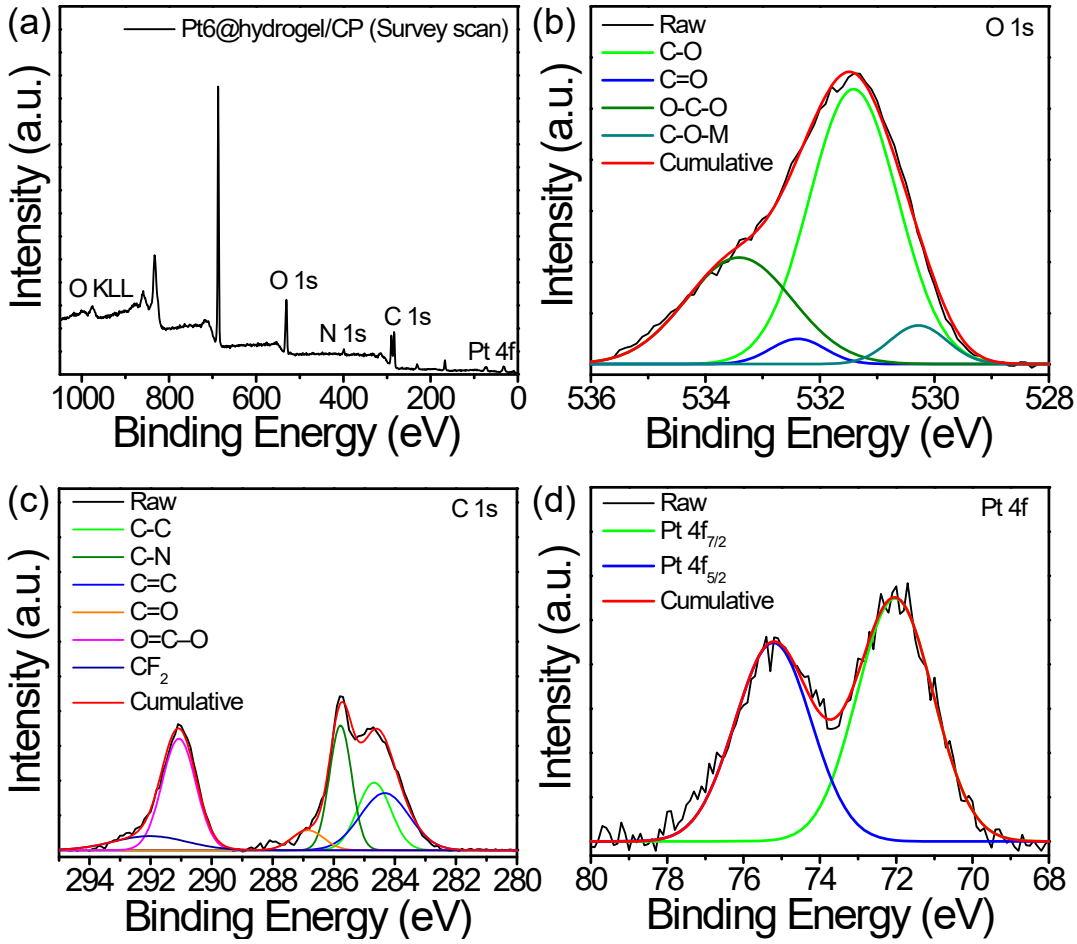

Figure S11. (a) XPS survey profile of Pt6@hydrogel/CP with the high-resolution profile of (b) O 1s, (c) C 1s, (d) Pt 4f after stability test.

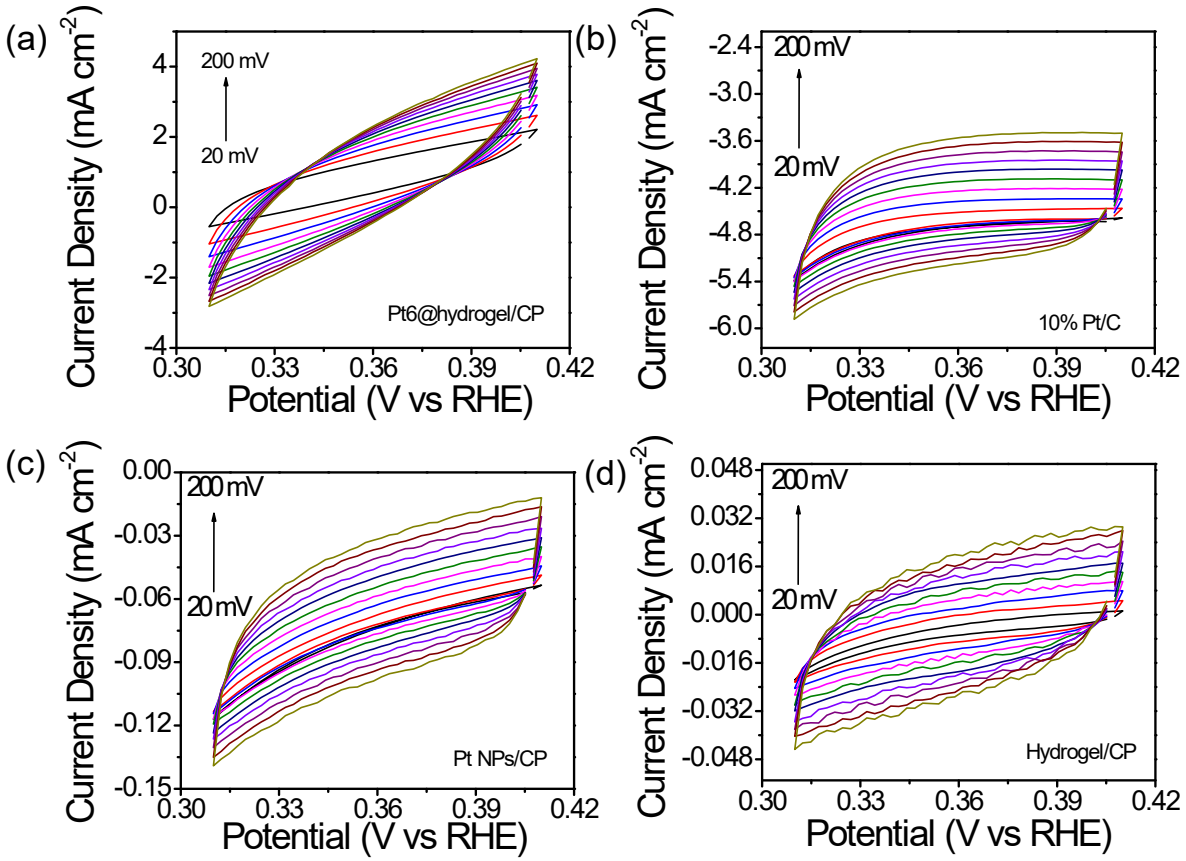

Figure S12. CV profiles of Pt6@hydrogel/CP, 10% Pt/C, Pt NPs/CP, and hydrogel/CP at different scan rate in 0.5 M H_2SO_4 solution.

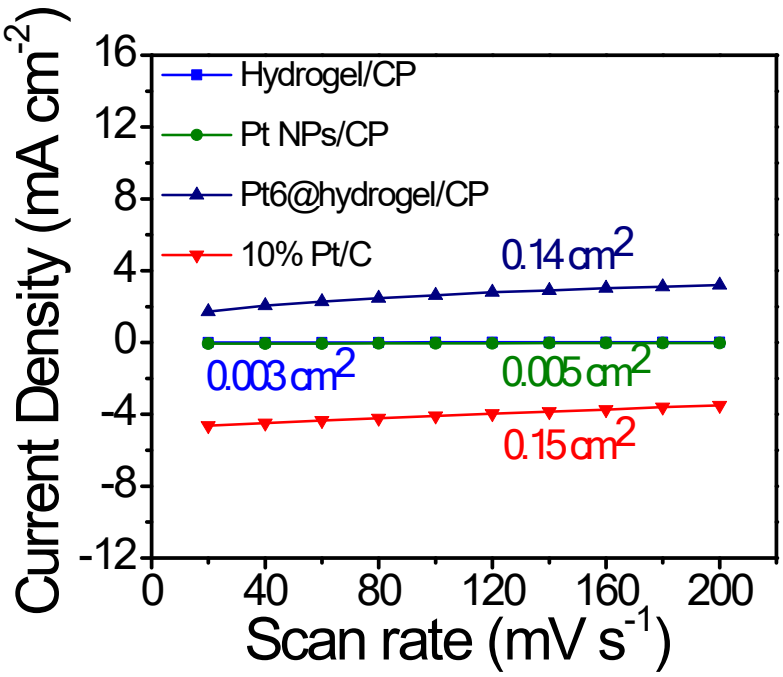

Figure S13. Linear relationship between capacitive current density at 0.38 V (vs RHE) and scan rate.

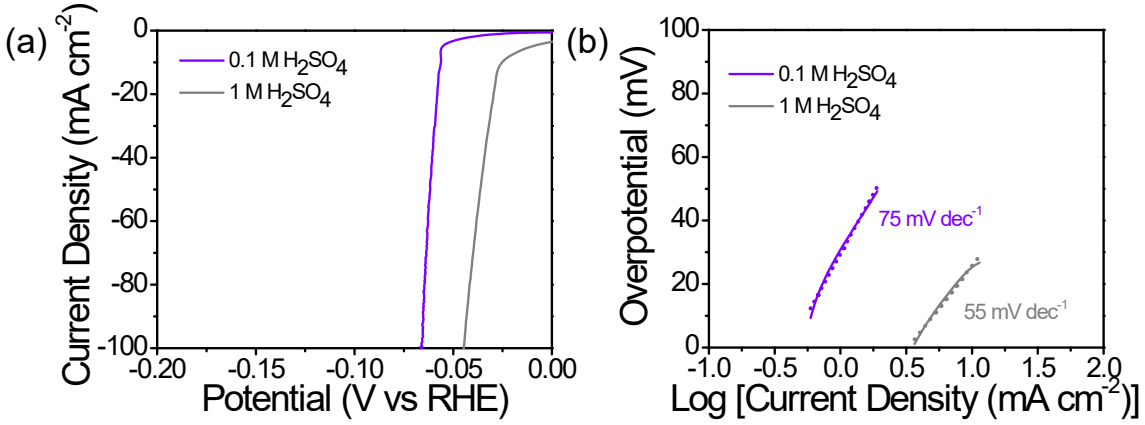

Figure S14. (a) iR-corrected LSV profiles of Pt6@hydrogel/CP scanned at 2 mV s^{-1} in 0.1 M H_2SO_4 and 1 M H_2SO_4, (b) respective Tafel slopes.

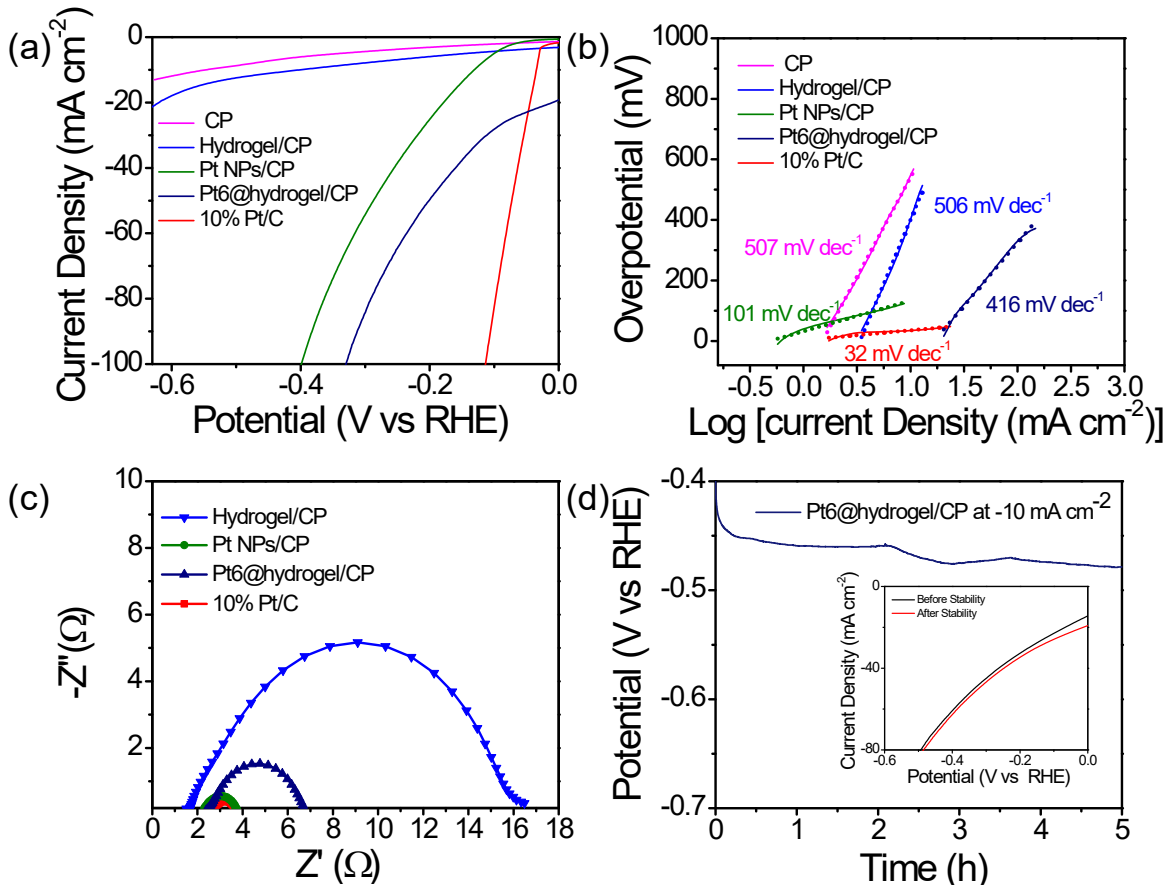

Figure S15. (a) iR-corrected LSV profiles of carbon paper (CP), hydrogel/CP, Pt NPs/CP, Pt6@hydrogel/CP and 10% Pt/C scanned at 2 mV s^{-1} in 1 M KOH solution, (b) respective Tafel slopes. (c) Nyquist plots of the prepared electrodes measured at a potential of -0.45 V. (d) The chronopotentiometry analysis of Pt6@hydrogel/CP for 5 h in 1 M KOH.

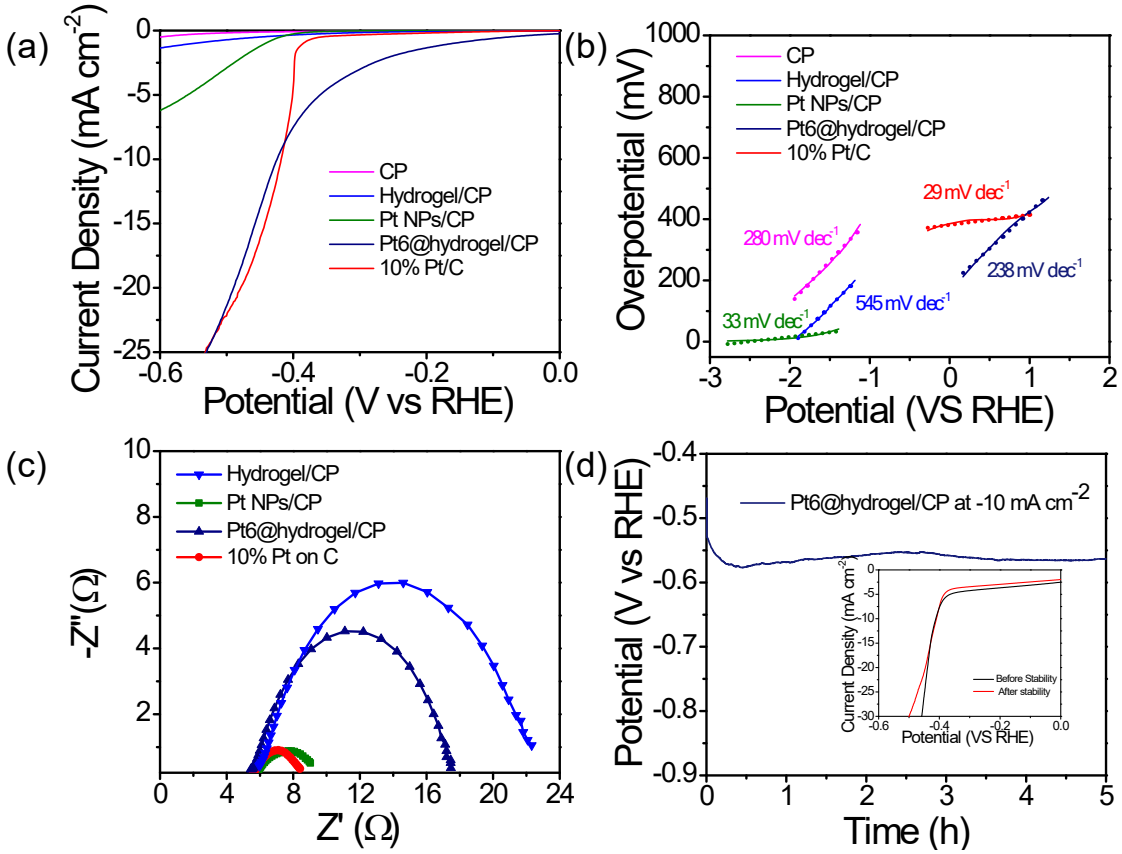

Figure S16. (a) iR-corrected LSV profiles of carbon paper (CP), hydrogel/CP, Pt NPs/CP, Pt6@hydrogel/CP and 10% Pt/C scanned at 2 mV s^{-1} in 1 M Phosphate buffer solution, (b) respective Tafel slopes. (c) Nyquist plots of the prepared electrodes measured at a potential of -0.45 V. (d) The chronopotentiometry analysis of Pt6@hydrogel/CP for 5 h in 1 M Phosphate buffer.

Table S2. HER performance of Pt2@hydrogel/CP, Pt4@hydrogel/CP, Pt6@hydrogel/CP, Pt8@hydrogel/CP in 0.5 M H_2SO_4 solution.

Catalyst	Electrolyte	Overpotential (mV) at 10 mA cm^{-2}	Tafel Slope	Pt Content (Loading)	R_{ct} (Ω)	ECSA (cm^2)
Pt2@hydrogel/CP	0.5 M H_2SO_4	140	81	0.070 mg	1.9	0.02
Pt4@hydrogel/CP	0.5 M H_2SO_4	133	76	0.126 mg	0.87	0.04
Pt6@hydrogel/CP	0.5 M H_2SO_4	45	52	0.168 mg	0.68	0.14
Pt8@hydrogel/CP	0.5 M H_2SO_4	136	77	0.304 mg	1.76	0.08

Table S3. HER performance of Pt6@hydrogel/CP, Pt NPs/CP and Pt/C in 0.5 M H_2SO_4 solution.

Catalyst	Electrolyte	Overpotential (mV) at 10 mA cm^{-2}	Tafel Slope	R_{ct} (Ω)	ECSA (cm^2)
Pt on C	0.5 M H_2SO_4	37	50	0.59	0.15
Pt6@hydrogel/CP	0.5 M H_2SO_4	45	52	0.68	0.14
Pt NPs	0.5 M H_2SO_4	117	144	2	0.005

Table S4. Comparative HER performance of Pt-based developed electrocatalysts.

Catalyst	**Overpotential at 10 mA cm^{-2} (mA)**	**Tafel Slope**	**Electrolyte**	**Pt Content (Loading)**	**Ref.**
3%Pt/WS_2	80	55	0.5 M H_2SO_4		4
Pt@Te-rGO	100	55	0.5 M H_2SO_4		68
PANI-Chito/Pt	450	121	0.5 M H_2SO_4		69
Pt@CNF	175	50	0.5 M H_2SO_4	7 wt%	70
Hollow Pt nanotube and nanosphere	27 and 31	21 and 23	0.5 M H_2SO_4	0.56mg/cm^2	71
PolyTT-Pt	67	37	0.5 M H_2SO_4	8.55 µg/cm^2	72
Ultralow Pt/BCF	55	32	0.5 M H_2SO_4	0.87 wt%	73
Pt6@hydrogel/CP	45	52	0.5 M H_2SO_4	0.168 mg/cm^2	This work

Table S5. HER performance of Pt6@hydrogel/CP, in 0.1 M H_2SO_4 and 1 M H_2SO_4 solution.

Catalyst	Electrolyte	Overpotential (mV) at 10 mA cm^{-2}	Tafel Slope
Pt6@hydrogel/CP	0.1 M H_2SO_4	56	75
Pt6@hydrogel/CP	1 M H_2SO_4	48	55

Table S6. HER performance of Pt6@hydrogel/CP, Pt NPs/CP and Pt/C in 1 M KOH solution.

Electrode	Overpotential (mV) at 10 mA cm^{-2}	Tafel Slope	R_{ct} (Ω)
Pt on C	34	32	0.6
Pt6@hydrogel/CP	140	416	4.2
Pt NPs/CP	131	101	1.8

Table S7. HER performance of Pt6@hydrogel/CP, Pt NPs/CP and Pt/C in 1 M Phosphate buffer solution.

Electrode	Overpotential (mV) at 10 mA cm^{-2}	Tafel Slope	R_{ct} (Ω)
Pt on C	418	29	3.8
Pt6@hydrogel /CP	424	238	9.1
Pt NPs/CP	491	33	4.1

^{1}H NMR and ^{13}C NMR data of all synthesized compounds:

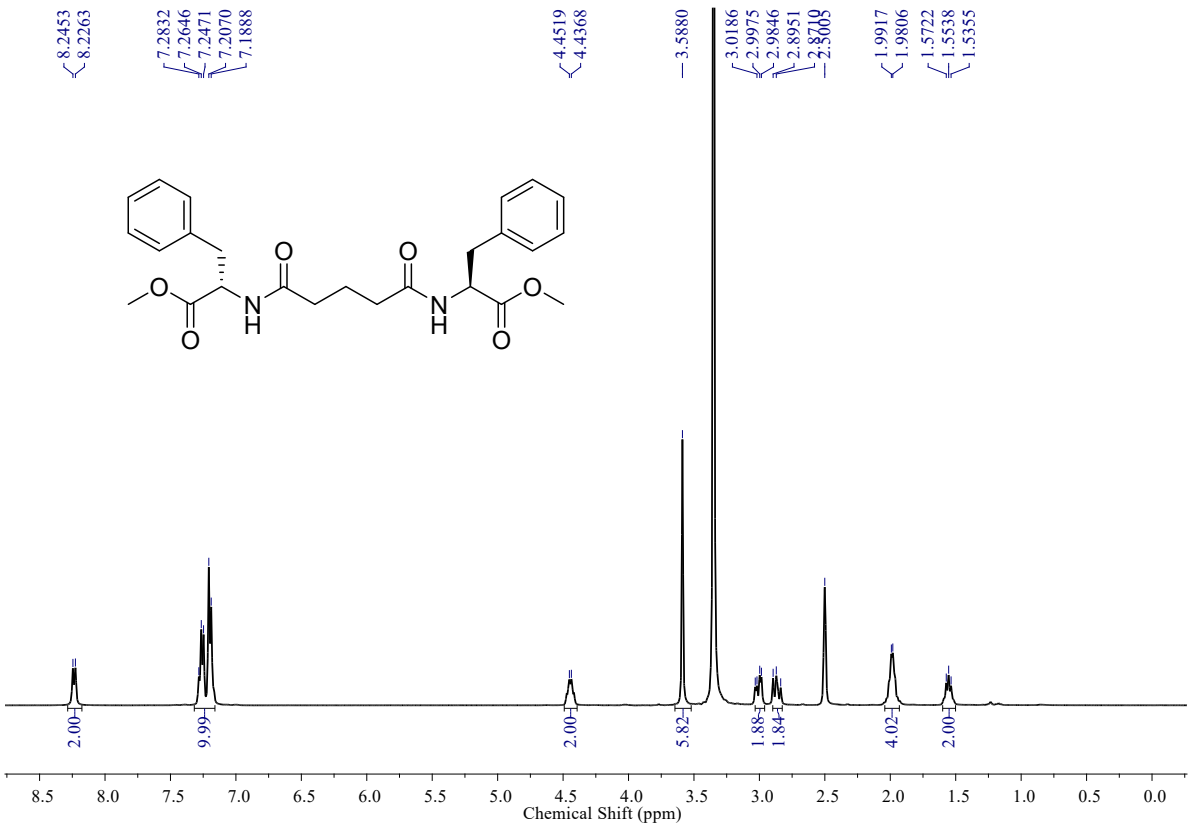

Figure S17. ^{1}H NMR (400 MHz, DMSO-d_6) spectrum of MeO-F-GluA-F-OMe **(4)**.

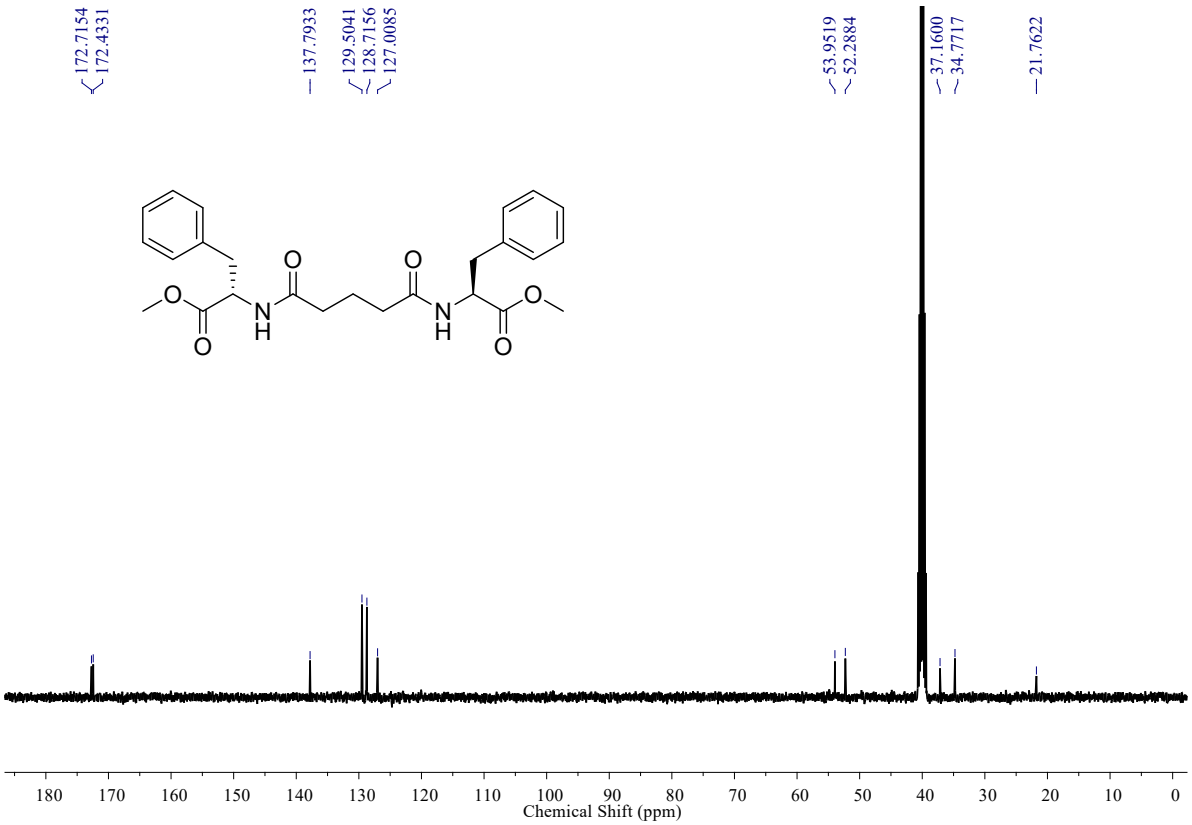

Figure S18. ^{13}C NMR (400 MHz, DMSO-d_6) spectrum of MeO-F-GluA-F-OMe **(4)**.

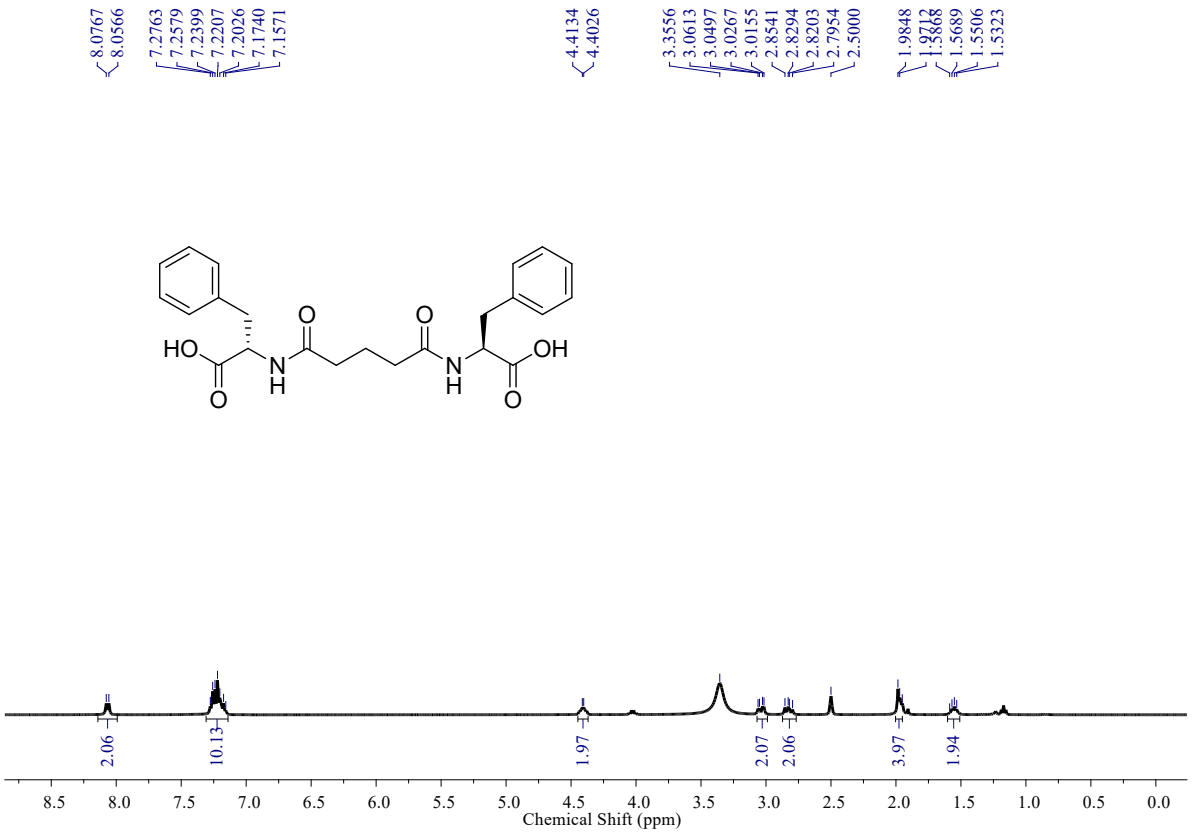

Figure S19. ^{1}H NMR (400 MHz, DMSO-d_6) spectrum of HO-F-GluA-F-OH **(5)**.

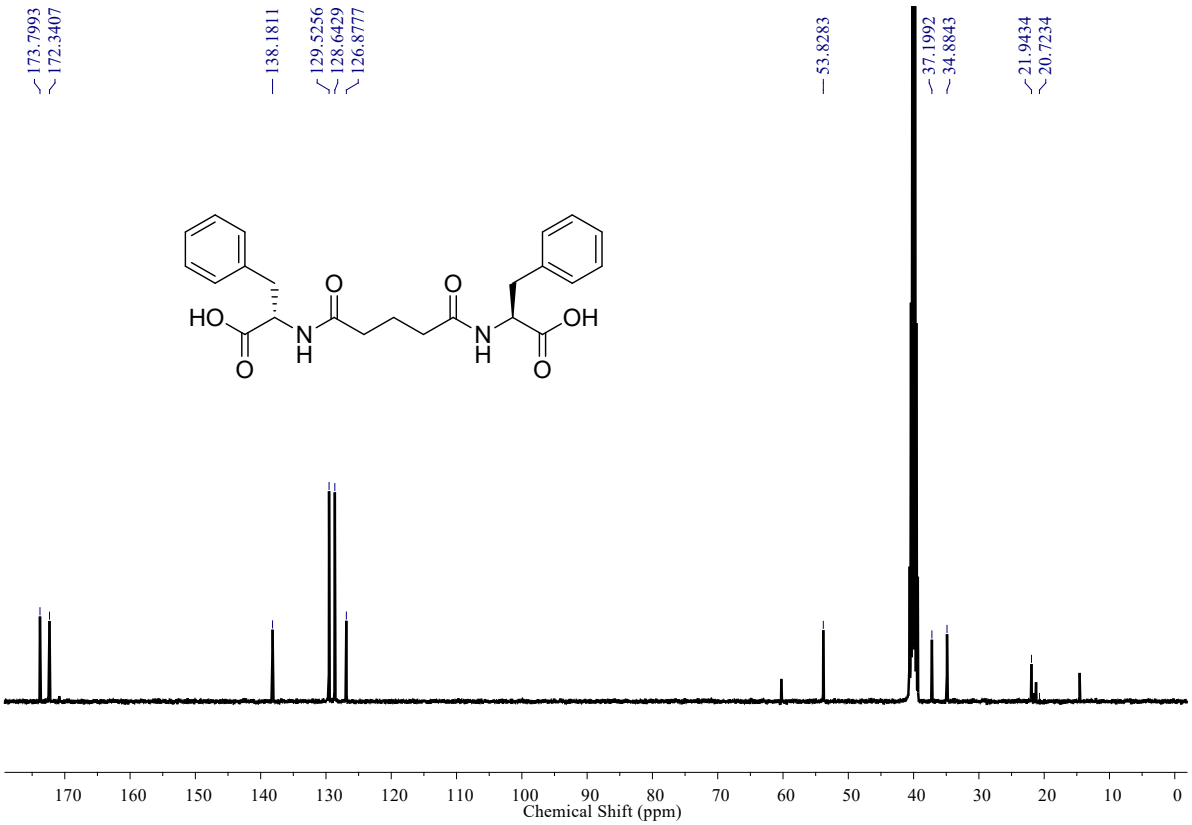

Figure S20. ^{13}C NMR (400 MHz, DMSO-d_6) spectrum of HO-F-GluA-F-OH **(5)**.

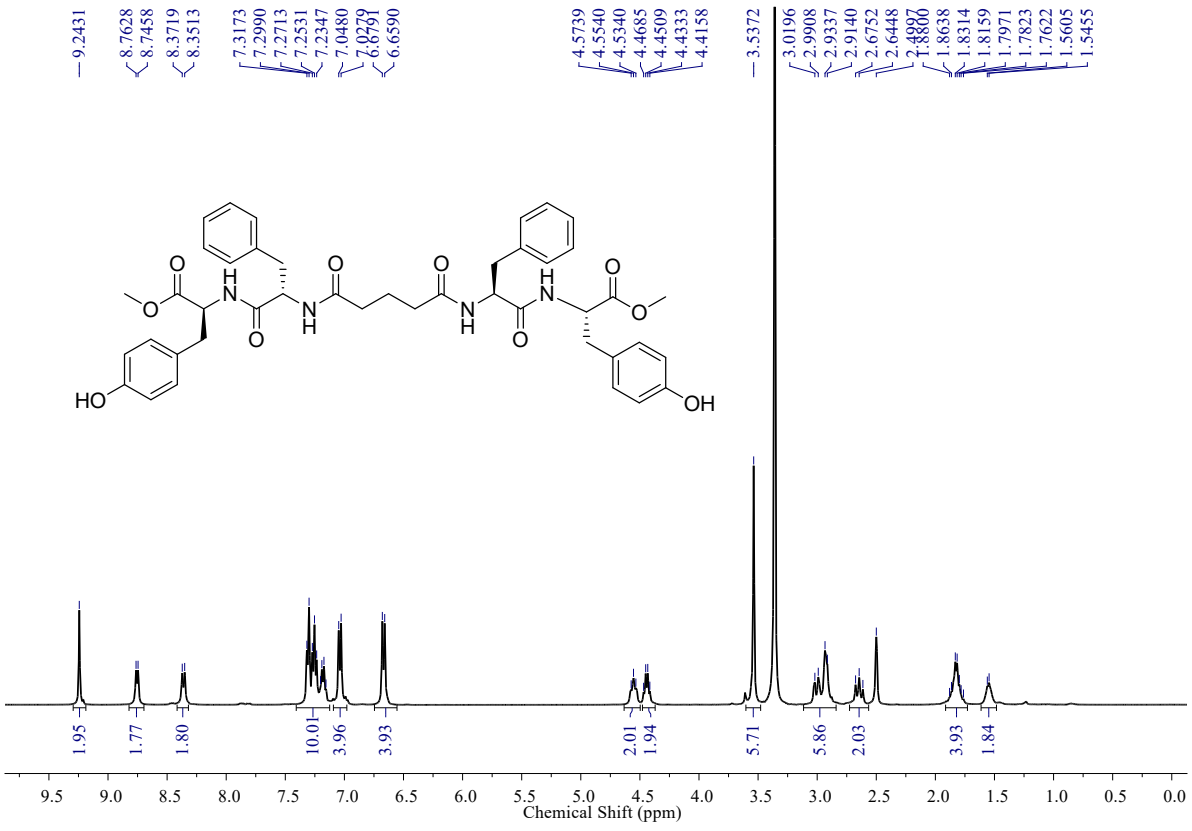

Figure S21. ^{1}H NMR (400 MHz, DMSO-d_6) spectrum of MeO-Y-F-GluA-F-Y-OMe **(7)**.

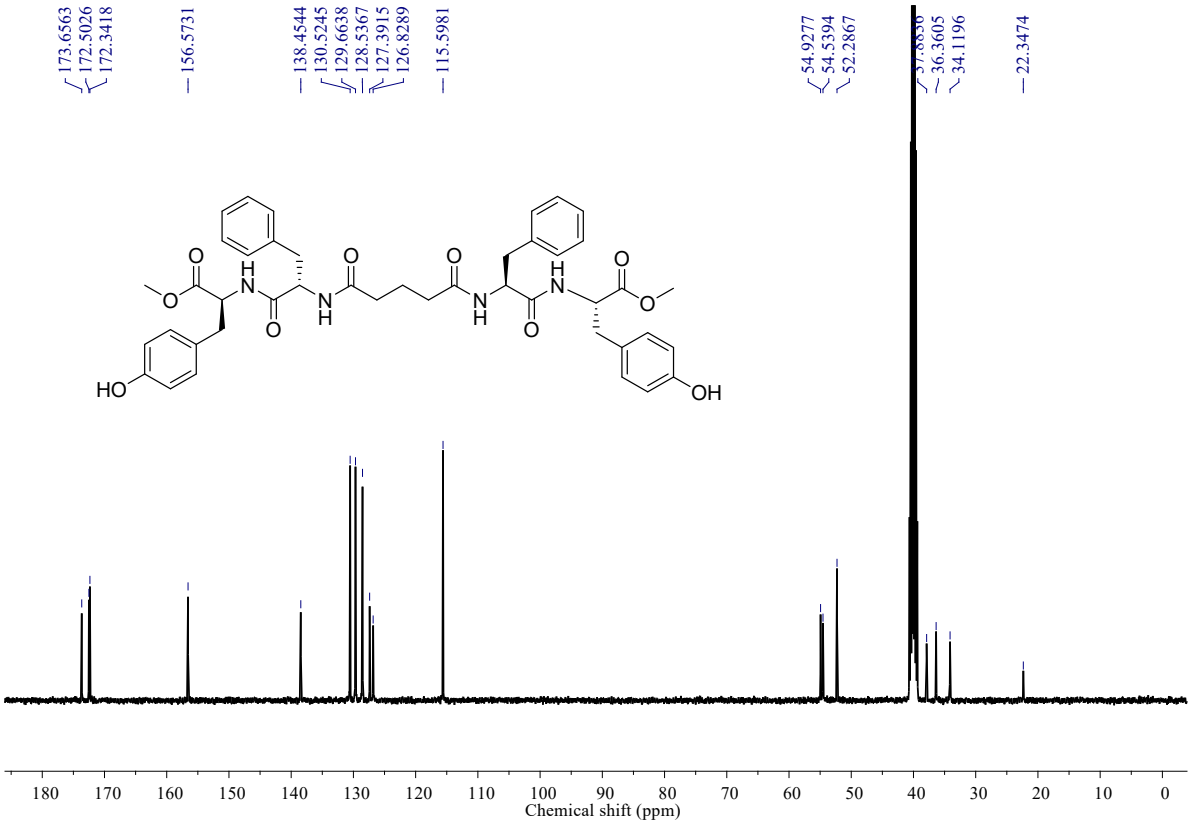

Figure S22. ^{13}C NMR (400 MHz, DMSO-d_6) spectrum of MeO-Y-F-GluA-F-Y-OMe **(7)**.

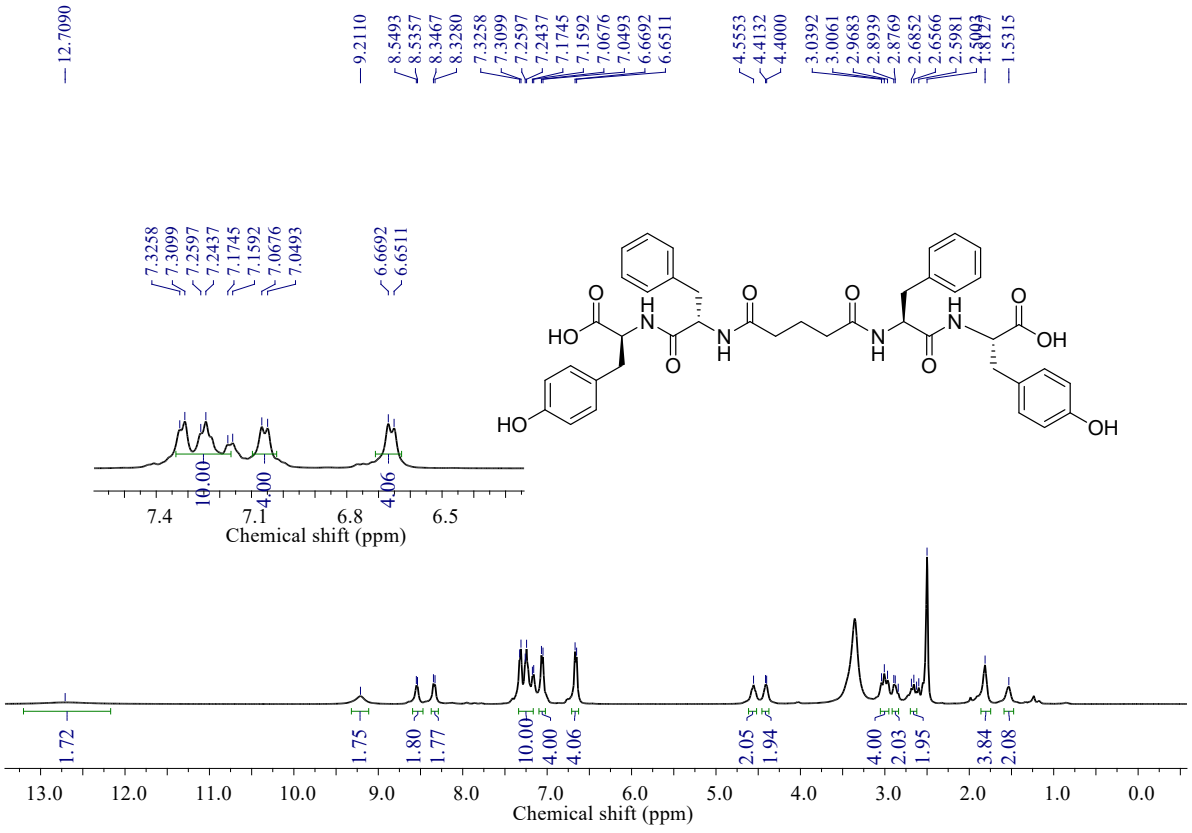

Figure S23. ^{1}H NMR (400 MHz, DMSO-d_6) spectrum of HO-Y-F-GluA-F-Y-OH **(1)**.

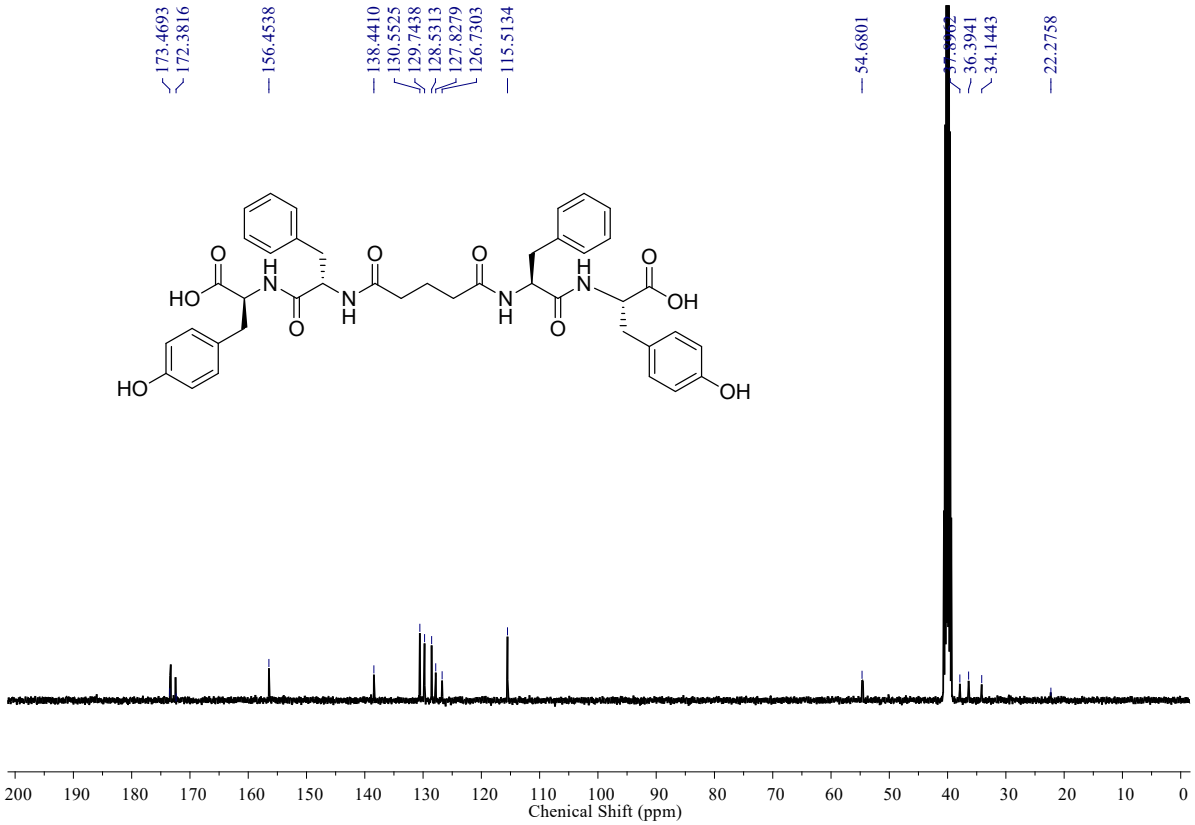

Figure S24. ^{13}C NMR (400 MHz, DMSO-d_6) spectrum of HO-Y-F-GluA-F-Y-OH **(1)**

Mass Spectrometry data of compounds:

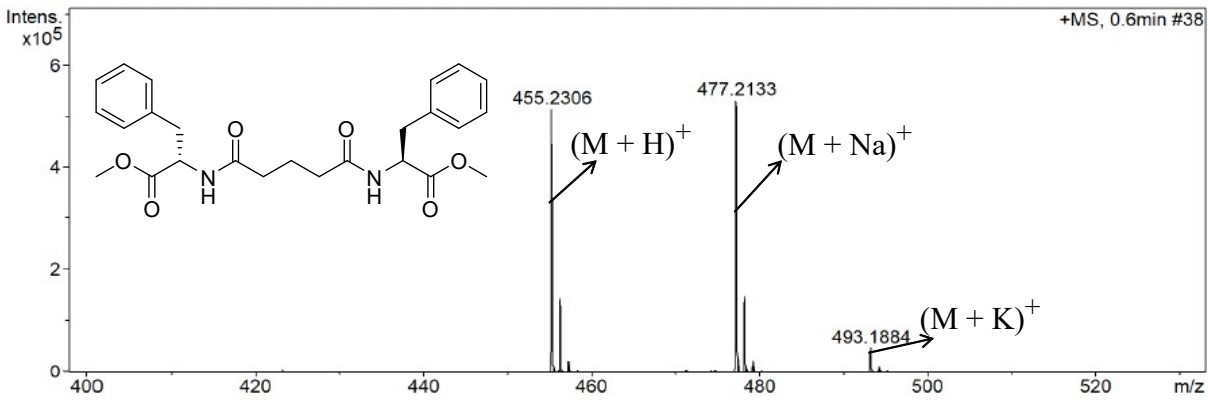

Figure S25. ESI-MS spectrum of MeO-F-GluA-F-OMe **(4)**

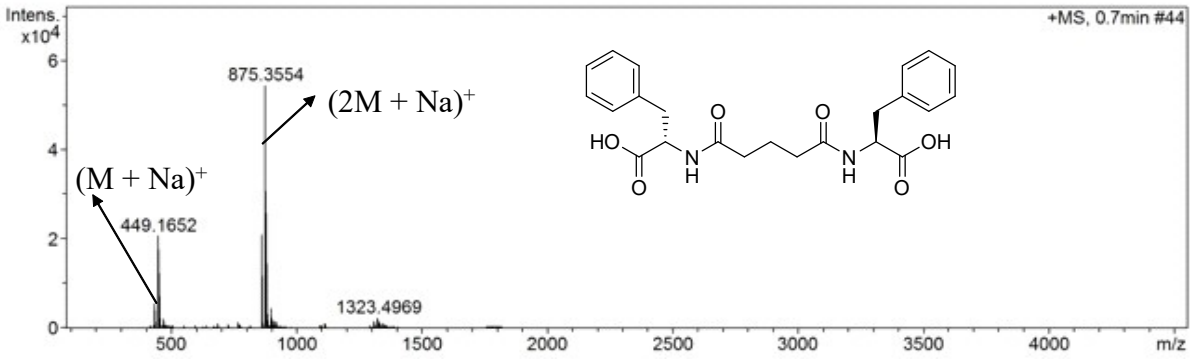

Figure S26. ESI-MS spectrum of HO-F-GluA-F-OH **(5)**.

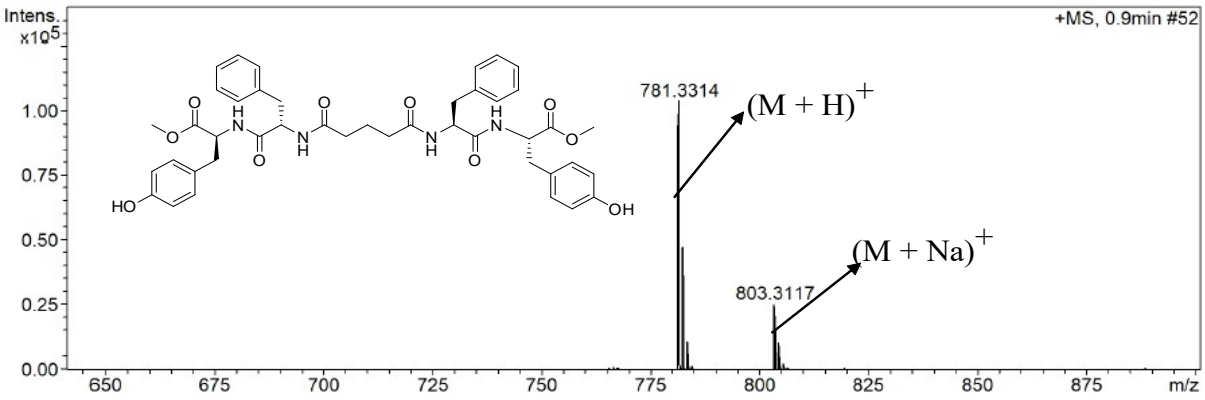

Figure S27. ESI-MS spectrum of MeO-Y-F-GluA-F-Y-OMe **(7)**.

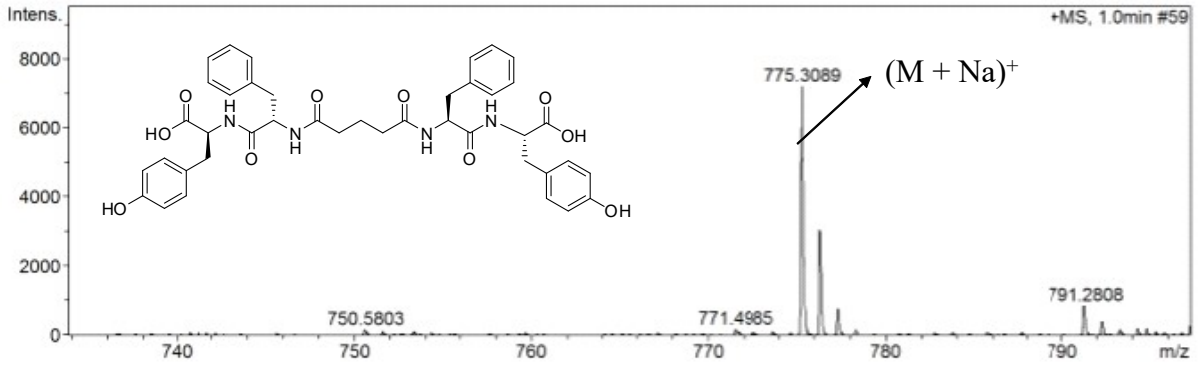

Figure S28. ESI-MS spectrum of HO-Y-F-GluA-F-Y-OH **(1)**.

References:

1 N. V. Long, M. Ohtaki, V. N. Ngo, M. T. Cao and M. Nogami, *Adv. Nat. Sci. Nanosci. Nanotechnol.*, 2012, **3**, 025005.

2 R. Bhandari, D. B. Pacardo, N. M. Bedford, R. R. Naik and M. R. Knecht, *J. Phys. Chem. C*, 2013, **117**, 18053–18062.